AGU PUBLICATIONS

Geophysical Research Letters

RESEARCH LETTER

10.1002/2013GL059026

Key Points:
- A thermophysical map of Vesta has been derived from spatially resolved data
- The average thermal inertia of the surface of Vesta is 30 ± 10 $Jm^{-2}s^{-0.5}K^{-1}$
- Pitted terrains in Marcia crater have the highest thermal inertia value

Supporting Information:
- Readme
- Text S1
- Figure S1
- Figure S2
- Figure S3
- Figure S4
- Figure S5
- Figure S6
- Figure S7
- Figure S8
- Figure S9
- Figure S10
- Figure S11

Correspondence to:
M. T. Capria,
mariateresa.capria@iaps.inaf.it

Citation:
Capria, M. T. et al. (2014), Vesta surface thermal properties map, *Geophys. Res. Lett.*, *41*, doi:10.1002/2013GL059026.

Received 12 DEC 2013
Accepted 17 FEB 2014
Accepted article online 19 FEB 2014

Vesta surface thermal properties map

M. T. Capria[1], F. Tosi[1], M. C. De Sanctis[1], F. Capaccioni[1], E. Ammannito[1], A. Frigeri[1], F. Zambon[1], S. Fonte[1], E. Palomba[1], D. Turrini[1], T. N. Titus[2], S. E. Schröder[3], M. Toplis[4], J.-Y. Li[5], J.-P. Combe[6], C. A. Raymond[7], and C. T. Russell[8]

[1]Istituto di Astrofisica e Planetologia Spaziali, INAF, Rome, Italy, [2]Astrogeology Science Center, U.S. Geological Survey, Flagstaff, Arizona, USA, [3]Deutsches Zentrum für Luft und Raumfahrt, Berlin, Germany, [4]Institut de Recherche en Astrophysique et Planétologie, Observatoire Midi-Pyrénées, Toulouse, France, [5]Department of Astronomy, University of Maryland, College Park, Maryland, USA, [6]Bear Fight Institute, Winthrop, Washington, USA, [7]Jet Propulsion Laboratory, California Institute of Technology, Pasadena, California, USA, [8]Institute of Geophysics and Planetary Physics, University of California, Los Angeles, California, USA

Abstract The first ever regional thermal properties map of Vesta has been derived from the temperatures retrieved by infrared data by the mission Dawn. The low average value of thermal inertia, 30 ± 10 J m^{-2} $s^{-0.5}$ K^{-1}, indicates a surface covered by a fine regolith. A range of thermal inertia values suggesting terrains with different physical properties has been determined. The lower thermal inertia of the regions north of the equator suggests that they are covered by an older, more processed surface. A few specific areas have higher than average thermal inertia values, indicative of a more compact material. The highest thermal inertia value has been determined on the Marcia crater, known for its pitted terrain and the presence of hydroxyl in the ejecta. Our results suggest that this type of terrain can be the result of soil compaction following the degassing of a local subsurface reservoir of volatiles.

1. Introduction and Background

Determining the thermal inertia of the surface of an atmosphere-less body provides insight into the structure and physical properties of that surface, giving indications on the type and history of the surface material [*Harris and Lagerros*, 2002]. However, our knowledge of asteroidal thermal properties is still based on relatively few data, mainly derived by disk-integrated measurements [see, e.g., *Delbo et al.*, 2011] which provide average results. Thermal inertia is a function of the thermal conductivity, the density, and thermal capacity of the material and depends on regolith particle size and depth, degree of compaction, exposure of rocks, and composition in the first centimeters of the surface. It is defined as $TI = \sqrt{K\rho c}$ (J m^{-2} $s^{-0.5}$ K^{-1}), where K is the thermal conductivity, ρ is the density, and c is the specific heat. It provides a quantified expression of how fast a material is able to store heat during the day and to release it at night. As such, it is the key property controlling surface temperature variations on airless bodies and is a sensitive indicator of the presence of dust, regolith, or rock, since these materials are more or less thermally insulating. In general, unconsolidated fines (i.e., dust) have low values of thermal inertia (5–30 J m^{-2} $s^{-0.5}$ K^{-1}) [*Putzig*, 2006]; sand-sized particles have higher values (i.e., about 400 J m^{-2} $s^{-0.5}$ K^{-1} for Mars [*Mellon et al.*, 2000] and a still higher value for an atmosphere-less body [*Presley and Christensen*, 1997]); and rocks and exposed bedrock have still higher values (even larger than 2500 J m^{-2} $s^{-0.5}$ K^{-1}) [*Jakosky*, 1986]. By considering thermal inertia together with other observed surface properties, insight can be gained into the physical characteristics of the surface and the geological processes by which the surface has been affected.

To derive the Vesta thermal properties map, the data acquired by the Visual and Infrared (VIR) [*De Sanctis et al.*, 2011] mapping spectrometer on Dawn [*Russell et al.*, 2012] have been used. VIR operates in the range 0.25–5.1 μm with an instantaneous field of view of 250 μrad. The region of the infrared spectrum between 3.5 and 5.1 μm is dominated by the thermal emission of the asteroid's surface. The measured radiance in this spectral region has been used to determine surface temperature and spectral emissivity by means of temperature retrieval algorithms [*Keihm et al.*, 2012].

The VIR spatially resolved data (1.3 km/pixel), obtained during the Approach phase at a heliocentric distance of 2.23 AU, have been the subject of the analysis discussed in this paper. The general behavior of surface temperature on a global scale is mainly determined by latitude, season, and local solar time. Superimposed on this general trend, smaller-scale variations can be due to local illumination conditions and to variations in

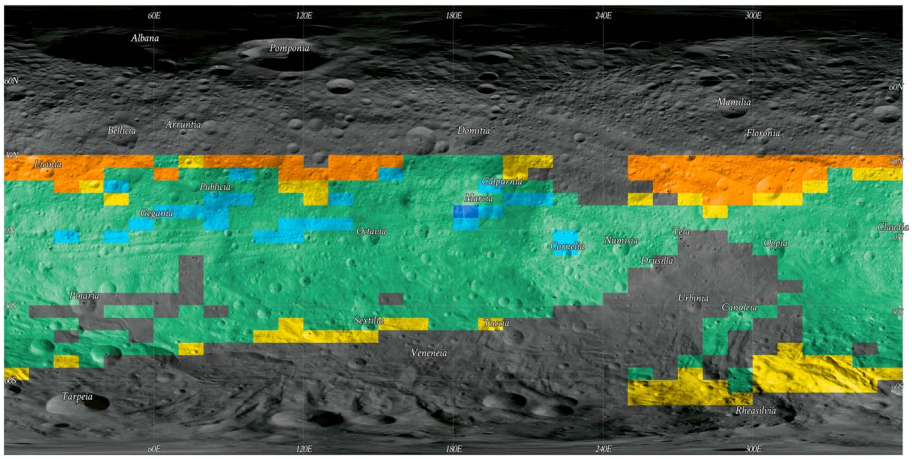

Figure 1. The thermal properties map of Vesta is superimposed on a Mercator projection map (in the Claudia coordinate system, here and in the rest of the paper, see http://sbn.psi.edu/archive/dawn/fc/DWNVFC2_1A/DOCUMENT/VESTA_COORDINATES/VESTA_COORDINATES_121214.PDF). Color code is as follows: blue, VHL class; light blue, HL class; green, AA class; yellow, LH class; and orange, VLH class.

the thermophysical properties in the first few centimeters of the Vestan soil. By comparing the measured temperatures with theoretical values, we observe that maximum temperature is fairly high and attained shortly after midday, both clear indications of a low thermal inertia.

2. Thermophysical Classification of the Surface of Vesta

2.1. The Thermophysical Model

In order to determine thermal inertia from measured temperatures, a thermophysical model is required. Our model solves the heat conduction equation and provides the temperature as a function of thermal conductivity, albedo, emissivity, and subpixel roughness $\bar{\xi}$ (see supporting information). Local illumination and observing geometry have been derived from the detailed shape model of Vesta [*Raymond et al*., 2011]. A layered terrain, with regolith on the surface and density increasing toward the interior, is assumed. Because night temperatures are unavailable (VIR is only sensitive to temperatures $>$ 180 K), it is impossible to reliably disentangle the effects of thermal conductivity and subpixel roughness. The subpixel roughness can be regarded as a measure of the surface irregularity at a scale smaller than the shape model (of the order of 20 m) and larger than the thermal skin depth (of the order of 1 cm, expressed, in the case of the diurnal cycle, as $D = \sqrt{KP/\pi\rho c}$, where P is the rotation period). It can be interpreted, for example, as the percentage of cratered terrain with respect to flat terrain [*Müller and Lagerros*, 1998; *Keihm et al*., 2012]. High values of the $\bar{\xi}$ parameter will increase the computed surface temperature, while low values, indicating a flatter surface, will have an opposite effect.

2.2. Derivation of the Thermal Properties Map

The procedure followed in order to derive the regional thermal inertia values is now described. The observed surface of Vesta has been divided in quadrangles of 5° latitude and 10° longitude. From the thermophysical code, theoretical temperature curves are computed representing the average temperatures, at the observation date, of each quadrangle, as a function of different values for the input parameters (thermal conductivity and subpixel roughness). Three classes of material with increasing thermal conductivity, from lunar dust to regolith, have been considered in the analysis. These parameters are changed, and the temperature is calculated iteratively until the best match with the measured temperatures is obtained. We were able to assign thermal inertia and subpixel roughness to most of the quadrangles in which the surface of Vesta has been divided, as shown in Figure 1.

The subpixel values given for each class are only indicative of a trend (high, average, and low); due to the unavailability of night temperatures, in many cases it is impossible to reliably disentangle the effects of thermal conductivity and subpixel roughness in the derivation of thermal inertia values.

Five different classes have been identified by their associated values of thermal inertia and subpixel roughness:

1. *Very low thermal inertia-high roughness* (*VLH*) (TI = 10 ± 5 J m^{-2} $s^{-0.5}$ K^{-1}, $\xi = 0.67 \pm 0.02$, orange in the map). This type of terrain is characterized by a lower-than-average thermal inertia, which can be associated with very fine, powdery material; this class covers almost uniformly all the longitudes in a belt located north of the equator (latitudes 20°N–30°N). It is worth noting that the oldest terrains of Vesta are found at these latitudes [*Marchi et al*., 2012].
2. *Low thermal inertia-high roughness* (*LH*) (TI = 20 ± 10 J m^{-2} $s^{-0.5}$ K^{-1}, $\xi = 0.67 \pm 0.02$, yellow in the map). This class is the third most abundant, and its major occurrence is correlated with terrains mainly located in the southernmost regions comprised between longitudes 240°E–360°E, close to the central pit of Rheasilvia.
3. *Intermediate thermal inertia-intermediate roughness* (*AA*) (TI = 30 ± 10 J m^{-2} $s^{-0.5}$ K^{-1}, $\xi = 0.44 \pm 0.02$, green in the map). This is the most abundant class, grouping regions mainly found around and immediately below the equator.
4. *High thermal inertia-low roughness* (*HL*) (TI = 40 ± 10 J m^{-2} $s^{-0.5}$ K^{-1}, $\xi = 0.2 \pm 0.02$, light blue in the map). The regions pertaining to this class are only found within the green region. Various areas with relatively high thermal inertia and low roughness are visible in the longitude range 0°–240°E; major regions are notably around the Marcia and Calpurnia craters (0°–20°N, 180°E–220°E), the region of the Cornelia crater (10°S–0°, 220°E–230°E), the region centered around the Publicia crater (0°–25°N, 60°E–100°E), and the region north of the Lucaria Tholus (5°S–5°N, 100°E–140°E). Two of these areas partially cover spots (on the Calpurnia and Cornelia craters), where patches of pitted terrain have been detected [*Denevi et al*., 2012].
5. *Very high thermal inertia-low roughness* (*VHL*) (TI = 50 ± 5 J m^{-2} $s^{-0.5}$ K^{-1}, $\xi = 0.2 \pm 0.02$, blue in the map). Only one quadrangle has been found with such a large thermal inertia value. This is roughly coincident with one of the more intriguing areas on the surface of Vesta, the Marcia crater (5°N–10°N, 180°E–190°E), where pitted terrain has been found [*Denevi et al*., 2012].

3. Discussion

The resulting picture is that the surface of Vesta is dominated by materials with a low thermal inertia. The best analog is probably the surface of the Moon, as depicted in *Vasavada et al*. [2012] and *Bandfield et al*. [2011]: a surface whose thermal response is determined by a widespread layer of dust and regolith with different grain sizes and density increasing toward the interior. Exposed rocks are probably scarce or even absent. The average thermal inertia of Vesta can be defined as 30 ± 10 J m^{-2} $s^{-0.5}$ K^{-1}, in good agreement with the values found by ground-based observations [*Müller and Lagerros*, 1998; *Chamberlain et al*., 2007; *Leyrat et al*., 2012].

The thermal inertia values derived from our analysis are not very different between them, but the surface of Vesta cannot be considered uniform from the point of view of thermal properties. The different thermal inertia and subpixel roughness values are suggestive of terrains with different physical properties, providing constraints that complement geological and mineralogical interpretations of other spectroscopic and/or morphological data of the Dawn mission.

It is interesting to note that the thermal inertia spatial distribution follows the global surface exposure ages distribution as determined by crater counting in *Raymond et al*. [2011]; the impact that generated the Rheasilvia crater caused a deep excavation in the Southern Hemisphere, totally obliterating any previous feature present in the crater area [*Schenk et al*., 2012] and giving rise to the youngest terrains on Vesta. Moving progressively away from the impact area, the blanketing due to the Rheasilvia event's ejecta has been less effective in masking the older terrains, thus giving weight to the association of northern regions with older terrains. The surface soil comminution is directly related to the materials' exposure times, and consequently very fine, dusty soil materials could explain the low thermal inertia regions prevailing north of the equator.

The other notable finding is related to the highest thermal inertia classes which are all located in the quadrangles falling in the longitude range 20°E–230°E and bounded in latitude between 10°S and 25°N. This region contains most of the quadrangles with the highest thermal inertia and is a low-albedo region [*Schröder et al*., 2013]. It is also the region of highest abundance of OH^{-}, as determined by the 2.8 μm band depth [*De Sanctis et al*., 2012b], and of hydrogen, as determined by the Gamma Ray and Neutron Detector

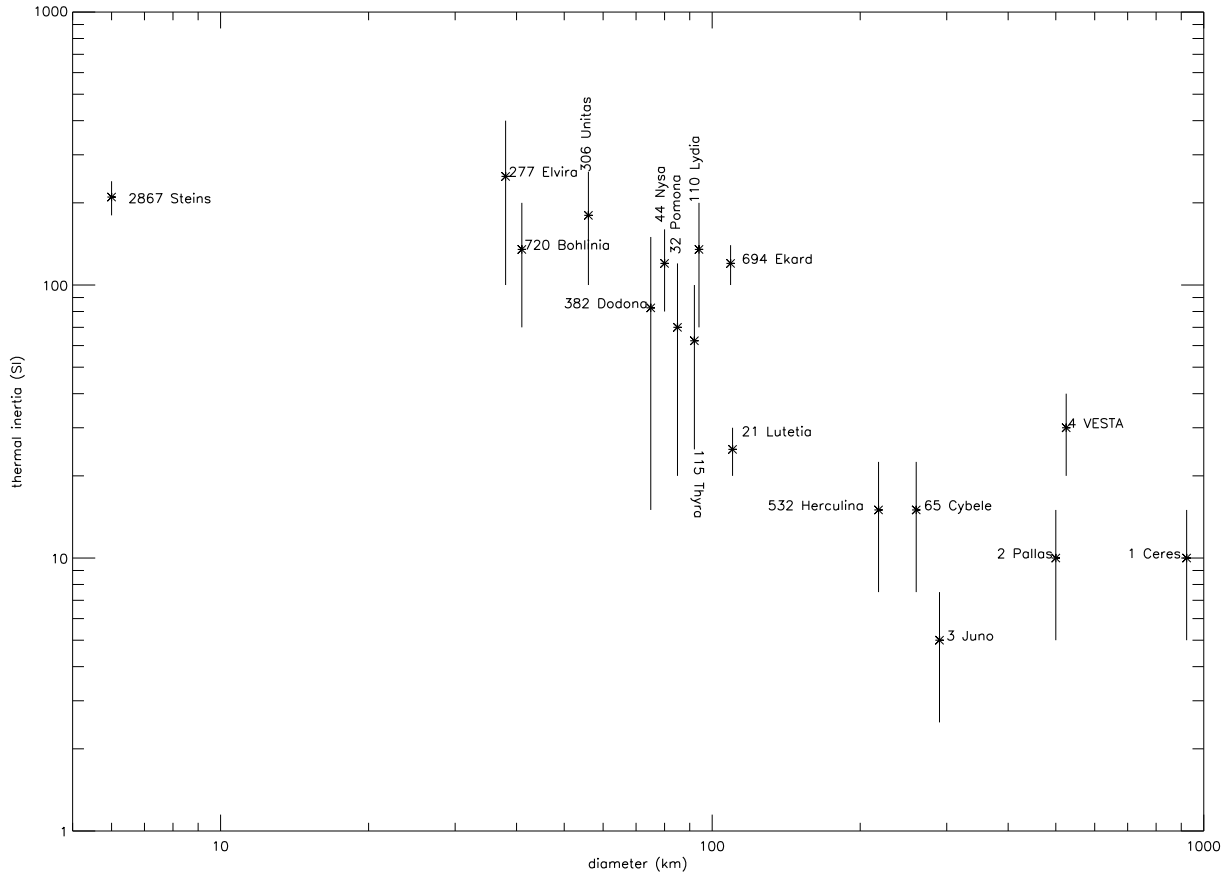

Figure 2. Thermal inertia of Main Belt asteroids with respect to the diameter: the data (with the exception of Vesta) are taken from literature [*Delbo and Tanga*, 2008; *Müller and Lagerros*, 1998; *Müller and Blommaert*, 2004; *Coradini et al*., 2011]. The thermal inertia of smaller (less than 100 km) asteroids is clearly higher than that of larger bodies, even taking into account the uncertainties due to the different techniques used to derive the results reported in the plot.

instrument [*Prettyman et al*., 2012]. Those observations are consistent with the delivery of water and hydrogen to Vesta's regolith by the infall of carbonaceous meteoroids and subsequent mixing of carbonaceous materials with the Vestan basaltic crust. The association of terrains rich in carbonaceous chondrite (CC) materials with areas of comparatively large thermal inertia is certainly suggestive but poses also a question. CCs have lower densities and lower thermal conductivity [*Opeil et al*., 2010] than basaltic material akin to howardite, eucrite, and diogenite meteorites. This consideration would point to a lower thermal inertia rather than a higher one, as observed on Vesta. Thus, the factor controlling the thermal inertia in these areas could be the degree of compaction of the uppermost surface layers, higher than in other parts of the surface.

This same consideration applies to the highest thermal inertia area, which is partly coincident with the Marcia crater (5°N–10°N, 180°E–190°E). This formation is well known for the pitted terrains in the crater floor and in the ejecta [*Denevi et al*., 2012] and OH^- presence mainly in the ejecta [*De Sanctis et al*., 2012a; *De Sanctis et al*., 2012b]. The terrain in this area seems to have different structural properties, probably a higher compactness level giving origin to higher thermal inertia values. Pitted terrains are a type of terrain, until now, besides Vesta, found only on Mars [*McEwen et al*., 2007] and are thought to be originated by the devolatilization of ice-rich material of possible exogenic origin.

Thermal inertia has been derived for a number of other Main Belt asteroids from ground- and space-based observations [*Delbo and Tanga*, 2008; *Müller and Lagerros*, 1998; *Müller and Blommaert*, 2004; *Coradini et al*., 2011]. At a global scale, Vesta's thermal inertia is much lower than that of small asteroids and, even if slightly higher, still compatible with that of the few large asteroids for which data exist, like 1 Ceres, 2 Pallas, 3 Juno, 65 Cybele, and 532 Herculina (Figure 2). The observed trend in diameter-thermal inertia [*Delbo and Tanga*, 2008] has been interpreted in terms of age and collisional evolution: large Main Belt asteroids, over hundreds

of millions of years of evolution and exposure to the space environment, have developed on the surface a fine regolith layer gardened by small impacts. This insulating surface layer is at the origin of the low thermal inertia values that seem to be typical of the larger Main Belt bodies. By contrast, smaller bodies can have quite different collisional histories, often being the final product of disruptive events. Small Main Belt asteroids have lower values of surface gravity, making it difficult to retain smaller particles. Coarser material, and even exposed bedrock, is probably not rare, resulting in more thermally conductive topmost layers, explaining the tendency for higher thermal inertia values in the case of smaller asteroids.

Vesta has many physical and petrologic characteristics, including thermal inertia closer to that of a small, airless planet or a large satellite than that of an asteroid [*Russell et al*., 2012; *Jaumann et al*., 2012]. The comparison with Mercury and Earth's Moon is thus appropriate in this context. The average value of thermal inertia that can be attributed to Mercury [*Morrison*, 1970] is 67 J m^{-2} s$^{-0.5}$ K^{-1}. The average thermal inertia that can be attributed to the Moon is instead around 35 J m^{-2} s$^{-0.5}$ [*Keihm*, 1984]. Being strongly dependent on temperature, thermal inertia of bodies orbiting far from the Main Belt cannot directly compare with the thermal inertia of asteroids. If we scale the Mercury and Moon thermal inertia to the heliocentric distance of Main Belt asteroids, their thermal inertia values are comparable or even lower than that of Vesta.

With respect to asteroids, planet-sized bodies have had a different evolutionary history, mainly driven by differentiation and tectonic evolution. Their global thermal inertia values are thus likely the result of averaging over areas with considerably different properties. For instance, on the Moon, values of thermal inertia higher than 1000 J m^{-2} s$^{-0.5}$ K^{-1} [*Bandfield et al*., 2011] can be found locally, at a scale much smaller than that of the data analyzed in this work. On Vesta, from the analysis of temperature images at higher resolution, a great variability is seen at a local scale, with different material deposits giving rise to a variety of temperature anomalies [*McCord et al*., 2012]. These anomalies in temperature could correspond to thermal inertia variations with respect to the surrounding areas, as in the case of Marcia crater.

Vesta certainly shares with Mercury and the Moon a complex evolutionary history, recorded also in its thermophysical properties. Similar to the Moon, Vesta shows thermal inertia variability on its surface, corresponding to differences in age, topography, composition, and albedo. Vesta is much more similar to an atmosphere-less planet than to a large asteroid. The diversity of Vesta and the high variability found in its surface thermal properties strongly point to its uniqueness in the general context of asteroids.

Acknowledgments

The VIR project is funded by the Italian Space Agency (ASI), ASI-INAF contract I/004/12/0. VIR was developed under the leadership of the Istituto di Astrofisica e Planetologia Spaziale (INAF-IAPS), Rome, Italy. The instrument was built by Selex-Galileo, Florence, Italy. Support of the Dawn Science, Instrument, Operations Teams, as well as of the Dawn at Vesta Participating Scientist program, is gratefully acknowledged. We also acknowledge the hard work carried out by Robert Gaskell in providing a detailed shape model that was used in this work to properly model the data. The data obtained by VIR are available at the Small Bodies Node of the Planetary Data System (http://sbn.pds.nasa.gov/).

The Editor thanks Joshua Bandfield and an anonymous reviewer for their assistance in evaluating this paper.

References

Bandfield, J. L., R. R. Ghent, A. R. Vasavada, D. A. Paige, S. J. Lawrence, and M. S. Robinson (2011), Lunar surface rock abundance and regolith fines temperatures derived from LRO Diviner Radiometer data, *J. Geophys. Res.*, *116*, E00H02, doi:10.1029/2011JE003866.

Chamberlain, M. A., A. J. Lovell, and M. V. Sykes (2007), Submillimeter lightcurves of Vesta, *Icarus*, *192*, 448–459, doi:10.1016/j.icarus.2007.08.003.

Coradini, A., et al. (2011), The surface composition and temperature of asteroid 21 Lutetia as observed by Rosetta/VIRTIS, *Science*, *334*, 492, doi:10.1126/science.1204062.

De Sanctis, M. C., et al. (2011), The VIR spectrometer, *Space Sci. Rev.*, *163*, 329–360, doi:10.1007/s11214-010-9668-5.

De Sanctis, M. C., et al. (2012a), Spectroscopic characterization of mineralogy and its diversity across Vesta, *Science*, *336*, 697, doi:10.1126/science.1219270.

De Sanctis, M. C., et al. (2012b), Detection of widespread hydrated materials on Vesta by the VIR Imaging Spectrometer on board the Dawn Mission, *Astrophys. J.*, *758*(L36), 5, doi:10.1088/2041-8205/758/2/L36.

Delbo, M., and P. Tanga (2008), Thermal inertia of main belt asteroids smaller than 100 km from IRAS data, *Planet. Space Sci.*, *257*, 259–265, doi:10.1016/j.pss.2008.06.015.

Delbo, M., et al. (2011), The cool surfaces of binary near-Earth asteroids, *Icarus*, *212*, 138–148, doi:10.1016/Icarus.2010.12.011.

Denevi, B., et al. (2012), Pitted terrain on Vesta and implications for the presence of volatiles, *Science*, *338*, 246, doi:10.1126/science.1225374.

Harris, A. W., and J. S. V. Lagerros (2002), Asteroids in the thermal infrared, *in Asteroids III*, edited by W. F. Bottke et al, pp. 205–218, Univ. of Arizona Press, Tucson, Ariz.

Jakosky, B. M. (1986), On the thermal properties of Martian fines, *Icarus*, *66*, 117–124, doi:10.1016/0019-1035(86)90011-4.

Jaumann, R., et al. (2012), Vesta's shape and morphology, *Science*, *336*, 687, doi:10.1126/science.1219122.

Keihm, S. J. (1984), Interpretation of the lunar microwave brightness temperature spectrum—Feasibility of orbital heat flow mapping, *Icarus*, *60*, 568–589, doi:10.1016/0019-1035(84)90165-9.

Keihm, S. J., et al. (2012), Interpretation of combined infrared, submillimeter, and millimeter thermal flux data obtained during the Rosetta fly-by of Asteroid (21) Lutetia, *Icarus*, *221*, 395–404, doi:10.1016/j.icarus.2012.08.002.

Leyrat, C., A. Barucci, T. Mueller, L. O'Rourke, I. Valtchanov, and S. Fornasier (2012), Thermal properties of (4) Vesta derived from Herschel measurements, *Astron. Astrophys.*, *539*, 154, doi:10.1051/0004-6361/201117793.

Marchi, S., et al. (2012), The violent collisional history of asteroid 4 Vesta, *Science*, *336*, 690, doi:10.1126/science.1218757.

McCord, T. B., et al. (2012), Dark material on Vesta from the infall of carbonaceous volatile-rich material, *Nature*, *491*, 83–86, doi:10.1038/nature11561.

McEwen, A. S., et al. (2007), A closer look at water-related geologic activity on Mars, *Science*, *317*, 1706, doi:10.1126/science.1143987.

Mellon, M. T., B. M. Jakosky, H. H. Kieffer, and P. R. Christensen (2000), High-resolution thermal inertia mapping from the Mars Global Surveyor Thermal Emission Spectrometer, *Icarus*, *148*, 437, doi:10.1006/icar.2000.6503.

Morrison, D. (1970), Thermophysics of the planet Mercury, *Space Sci. Rev.*, *11*, 271–307, doi:10.1007/BF00241524.
Müller, T. G., and J. S. V. Lagerros (1998), Asteroids as far-infrared photometric standards for ISOPHOT, *Astron. Astrophys.*, *338*, 340–352.
Müller, T. G., and J. A. Blommaert (2004), 65 Cybele in the thermal infrared: Multiple observations and thermophysical analysis, *Astron. Astrophys.*, *418*, 347–356.
Opeil, C. P., G. J. Consolmagno, and D. T. Britt (2010), The thermal conductivity of meteorites: New measurements and analysis, *Icarus*, *208*, 449–454, doi:10.1016/j.icarus.2010.01.021.
Presley, M. A., and P. R. Christensen (1997), Thermal conductivity measurements of particulate materials 2. Results, *J. Geophys. Res.*, *102*, 6551–6566, doi:10.1029/96JE03303.
Prettyman, T. H., et al. (2012), Elemental mapping by Dawn reveals exogenic H in Vesta's regolith, *Science*, *338*, 242, doi:10.1126/science.1225354.
Putzig, N. E. (2006), Thermal inertia and surface heterogeneity on Mars. Ph.D. dissertation, Univ. of Colorado.
Raymond, C. A., et al. (2011), The Dawn topography investigation, *Space Sci. Rev.*, *163*, 487–510, doi:10.1007/s11214-011-9863-z.
Russell, C. T., et al. (2012), Dawn at Vesta: Testing the protoplanetary paradigm, *Science*, *336*, 684, doi:10.1126/science.1219381.
Schenk, P., et al. (2012), The geologically recent giant impact basins at Vesta's south pole, *Science*, *336*, 694, doi:10.1126/science.1223272.
Schröder, S. E., S. Mottola, H. U. Keller, C. A. Raymond, and C. T. Russell (2013), Resolved photometry of Vesta reveals physical properties of crater regolith, *Planet. Space Sci.*, *85*, 198–213, doi:10.1016/j.pss.2013.06.009.
Vasavada, A. R., J. L. Bandfield, B. T. Greenhagen, P. O. Hayne, M. A. Siegler, J.-P. Williams, and D. A. Paige (2012), Lunar equatorial surface temperatures and regolith properties from the Diviner Lunar Radiometer experiment, *J. Geophys. Res.*, *117*, E00H18, doi:10.1029/2011JE003987.